Astronomy & Astrophysics manuscript no. 18210
October 31, 2018
© ESO 2018

arXiv:1111.3250v1 [astro-ph.SR] 14 Nov 2011

VLT/X-shooter observations and the chemical composition of cool white dwarfs ⋆

Adéla Kawka[1,2] and Stéphane Vennes[1,2]

[1] Astronomický ústav, Akademie věd České republiky, Fričova 298, CZ-251 65 Ondřejov, Czech Republic
e-mail: kawka,vennes@sunstel.asu.cas.cz
[2] Visiting Astronomer, Cerro Tololo Inter-American Observatory, National Optical Astronomy Observatory, which are operated by the Association of Universities for Research in Astronomy under cooperative agreement with the National Science Foundation.

Received; accepted

ABSTRACT

We present a model atmosphere analysis of cool hydrogen-rich white dwarfs observed at the Very Large Telescope (VLT) with the X-shooter spectrograph. The intermediate-dispersion and high signal-to-noise ratio of the spectra allowed us to conduct a detailed analysis of hydrogen and heavy element line profiles. In particular, we tested various prescriptions for hydrogen Balmer line broadening parameters and determined the effective temperature and surface gravity of each star. Three objects (NLTT 1675, 6390 and 11393) show the presence of heavy elements (Mg, Al, Ca, or Fe). Our abundance analysis revealed a relatively high iron to calcium ratio in NLTT 1675 and NLTT 6390. We also present an analysis of spectropolarimetric data obtained at the VLT using the focal reducer and low dispersion spectrograph (FORS) and we established strict upper limits on the magnetic field strengths in three of the DAZ white dwarfs and determined the longitudinal magnetic field strength in the DAZ NLTT 10480. The class of DAZ white dwarfs comprises objects that are possibly accreting material from their immediate circumstellar environment and the present study contributes in establishing class properties.

Key words. white dwarfs – stars: atmospheres – stars: abundances – stars: magnetic field

1. Introduction

Studies of heavy elements in cool hydrogen-rich (DA) white dwarfs were originally restricted to a few cases, i.e., the cool white dwarf G74-7 (Lacombe et al., 1983) and the ZZ Ceti star G29-38 (Koester et al., 1997), because of their rarity. Diffusion timescales in cool DA white dwarfs are relatively short (Paquette et al., 1986), and heavy elements were not expected to be detectable in the photosphere of these objects. Therefore, heavy elements such as calcium in G74-7 must be continuously supplied from an external source. Incidentally, Zuckerman & Becklin (1987) reported an infrared excess in G29-38, and Graham et al. (1990) showed that the excess is caused by the presence of circumstellar dust. The detection of heavy elements (Mg, Ca, Fe) in the atmosphere of G29-38 by Koester et al. (1997) strengthened the link between atmospheric contaminants and the presence of circumstellar material.

Surveys of white dwarfs conducted using high-dispersion spectrographs attached to large aperture telescopes (e.g., Zuckerman et al., 1998, 2003; Koester et al., 2005) reveal that, contrary to earlier assessments, a significant fraction of DA white dwarfs, labelled DAZ white dwarfs, are contaminated with elements heavier than helium. Within a sample of $\sim$ 100 DA white dwarfs that are not in close binary systems, Zuckerman et al. (2003) showed that $\approx$ 25% of the stars exhibit photospheric heavy element lines; for the majority of stars in their sample only calcium lines are observed, but in some cases other elements such as magnesium, iron, aluminium and silicon are also detected.

Our study of cool white dwarfs in the revised NLTT catalogue (Salim & Gould, 2003) unveiled new cases of external contaminations. The stars were selected using a reduced proper motion diagram combined with optical and infrared colours (Kawka et al., 2004) resulting in a catalogue of $\approx$ 400 objects; only about half of these objects had previously been spectroscopically confirmed as white dwarfs. Although the NLTT catalogue is deemed incomplete at low Galactic latitude and far south (see Lépine & Shara, 2005), it still contains many stars that remain largely unstudied. More complete catalogues utilizing the Digital Sky Surveys, such as the LSPM catalogue of stars with proper motions greater than 0.15" yr^{-1} (Lépine & Shara, 2005) have been compiled and complement the NLTT catalogue where it is incomplete.

Kawka & Vennes (2006) conducted low-dispersion spectroscopic observations of white dwarf candidates from the NLTT catalogue and listed 49 new objects including 30 DA white dwarfs, three DAZ white dwarfs including NLTT 43806, and 16 non-DA white dwarfs. In following-up on NLTT 43806, Zuckerman et al. (2011) obtained high signal-to-noise and high-dispersion spectra showing it to harbour a weak magnetic field.

In this work, we present intermediate-dispersion and high signal-to-noise (S/N) ratio spectroscopy and a model atmosphere analysis of new DAZ white dwarfs that were selected from the New Luyten Two-Tenths (NLTT) catalogue. These new objects add to the few hydrogen-rich white dwarfs that have been scrutinized for heavy elements other than calcium. We presented a first report on this programme with the analysis of the coolest DAZ in our sample (NLTT 10480; Kawka & Vennes, 2011). The

⋆ Based on observations collected at the European Organisation for Astronomical Research in the Southern Hemisphere, Chile under programme ID 080.D-0521, 082.D-0750, 083.D-0540, 084.D-0862 and 086.D-0562.

Table 1. Log of spectroscopic observations

NLTT	Instrument	UT Date	Exp. Time (s)
1675	NTT/EFOSC2	2009 Aug. 24	2×1500
	VLT/X-shooter	2010 Nov. 13	2×2400
		2010 Dec. 8	2×2400
6390	VLT/FORS1	2007 Nov. 1	2×1500
	VLT/X-shooter	2011 Jan. 1	1×2400
11393	VLT/FORS1	2007 Nov. 3	2×1260
	NTT/EFOSC2	2008 Oct. 21	2×1200
	VLT/X-shooter	2010 Nov. 13	2×2400
		2011 Jan. 11	2×2400
23966	CTIO/R-C Spec	2008 Feb. 25	2×2400
	VLT/FORS2	2010 Jan. 23	4×1200
	VLT/X-shooter	2011 Jan. 6	1×1800
		2011 Jan. 30	1×1800
		2011 Mar. 26	1×1800

X-shooter spectrum of NLTT 10480 showed Zeeman-split calcium and hydrogen lines that revealed a surface magnetic field of $B_s = 0.519 \pm 0.004$ MG. At the present time, only three other magnetic DAZ white dwarfs are known: G77-50 (Farihi et al., 2011), NLTT 43806 (Zuckerman et al., 2011) and LTT 8381 (Koester et al., 2009). Apart from these four magnetic DAZ white dwarfs, two more white dwarfs with helium dominated atmospheres that are contaminated with heavy elements have also been shown to be weakly magnetic: G165-7 (Dufour et al., 2006) and LHS 2534 (Reid et al., 2001). Recently, Potter & Tout (2010) and Nordhaus et al. (2011) have proposed that magnetic fields in white dwarfs may be generated during the common-envelope phase of interacting binaries. Applying this model to the case of G77-50, Farihi et al. (2011) proposed that the presence of a weak field in this star may be the result of a past common-envelope episode with a planetary component during the white dwarf's formative years.

In the following Sect. 2 we describe observations obtained at the European Southern Observatories (ESO) using the New Technology Telescope (3.6-m) and the Very Large Telescopes (VLTs) as well as the 4-m telescope at Cerro Tololo Inter-American Observatory (CTIO). Sect. 3 presents our model atmosphere analysis including details of the model structure (Sect. 3.1) and heavy-element line profile (Sect. 3.2) calculations. Using these models we determine the effective temperature and surface gravity for each star (Sect. 3.3), and measure their heavy element abundance (Sect. 3.4). The stellar radial velocities and kinematics, and estimates of the magnetic field strengths are presented in Sect. 3.5 and Sect. 3.6, respectively. We summarize and discuss some implications of our results in Sect. 4.

2. Observations

2.1. Spectroscopy

We first observed objects from the present sample during a programme aimed at identifying new white dwarfs in the NLTT catalogue. NLTT 6390 and NLTT 11393 were observed with the focal reducer and low dispersion spectrograph (FORS1) attached to the 8m UT2 (Kuenyen) at Paranal Observatory on UT 2007 November 1 and 3 as part of our spectropolarimetric survey of white dwarfs. The purpose of these observations was to confirm the nature of the observed sample of stars and to search for weak magnetic fields. We used the 600B grism combined with a slit-width of 1 arcsecond that provided a resolution of 6 Å and a spectral range of 3780 to 6180 Å. The observations consisted of a sequence of two consecutive exposures. In the first exposure the Wollaston prism is rotated to $-45°$ followed by a second exposure with the Wollaston prism rotated to $+45°$ from which we extracted the flux and circular polarization spectra.

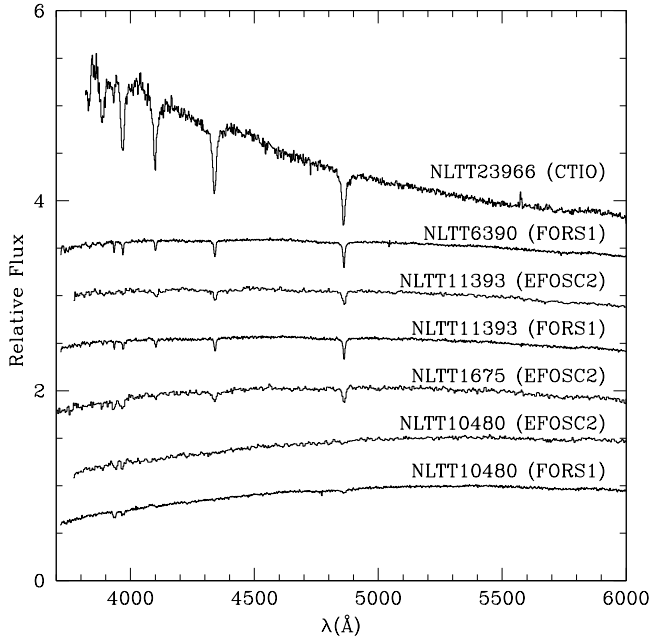

Fig. 1. Identification spectra, f_λ versus λ, normalized at λ = 5500Å and shifted up for clarity.

As part of our identification programme we observed NLTT 23966 with the R-C spectrograph attached to the 4m telescope at CTIO on UT 2008 February 25. We used the KPGL2 (316 lines per mm) grating with the WG360 filter to block out the second order contamination. We set the slit-width to 1.5 arcseconds which provided a spectral resolution of $\sim$ 8 Å and a spectral range of 3820 to 7500 Å. The spectra were flux calibrated with the flux standard GD 108. We also selected a sample of spectroscopically confirmed hydrogen-rich white dwarfs from the NLTT catalogue, including NLTT 23966, for spectropolarimetric observations with the aim of searching for weak magnetic fields. NLTT 23966 was observed with the FORS2 attached to the 8m UT1 (Antu) at Paranal Observatory on UT 2010 Jan 23. We used the 1200R grism with the order blocking filter GG435 and 2kx4k MIT CCD. The slit-width was set to 1 arcsecond which resulted in a spectral resolution of $\sim$ 3 Å and a spectral range of 5810 to 7290 Å. The observations were carried out in the same way as for NLTT 6390 and NLTT 11393 with the FORS1 spectrograph with one sequence consisting of two consecutive exposures with the Wollaston prism rotated 90° between the two exposures. Two sequences were obtained for NLTT 23966.

NLTT 1675 was first observed with the ESO Faint Object Spectrograph and Camera (EFOSC2) attached to the 3.6m New Technology Telescope (NTT) at La Silla Observatory on UT 2009 August 24. We used Grism 11 which has 300 lines per mm and a blaze wavelength of 4000 Å. The slit-width was set to 1 arcsecond which resulted in a spectral resolution of $\sim$ 14 Å and a spectral range of 3700 to 7250 Å. We have also observed NLTT 11393 using this setup on UT 2008 October 21. The ob-

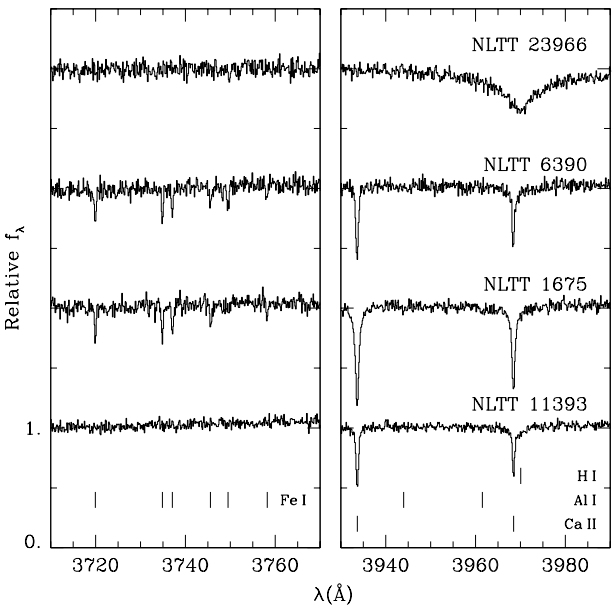

Fig. 2. X-shooter spectra covering iron (*left*) and calcium (*right*) lines in four cool, hydrogen-rich white dwarfs from the NLTT catalogue. Photospheric calcium lines are observed in three stars, while iron is only observed in NLTT 1675 and 6390. Contrary to our initial report (Kawka et al., 2011), our new X-shooter spectra show that NLTT 23966 is devoid of calcium. The possible identification of aluminium in reported for NLTT 1675.

servations were carried out at the parallactic angle and were flux calibrated with the flux standard Feige 110.

Figure 1 shows the low-dispersion identification spectra of the five cool hydrogen rich white dwarfs for which higher dispersion spectra were obtained with VLT/X-shooter, including the identification spectra of the cool magnetic DAZ NLTT 10480 which was analyzed by Kawka & Vennes (2011). The low dispersion spectra of these stars showed the presence of the Ca IIλ3933Å line and therefore were selected for follow-up high-dispersion observations with X-shooter. In the case of NLTT 23966 the Ca IIλ3933Å line seen in the CTIO spectrum was the result of background noise.

Following-up on our low-dispersion spectroscopic observations, we obtained a set of echelle spectra for all five objects (including NLTT 10480) using the X-shooter spectrograph attached to the UT2 (Kueyen) at Paranal Observatory (Vernet et al., 2011). The spectra were obtained with the slit-width set to 0.5, 0.9 and 0.6 arcsecond for the UVB, VIS and NIR arms, respectively. This set-up delivered a resolving power of 9100 for UVB, 8800 for VIS and 6200 for NIR.

Figure 2 shows X-shooter spectra of NLTT 1675, 6390, 11393 and 23966. Photospheric lines of calcium, iron and aluminium are marked. Table 1 summarizes our spectroscopic observations and Table 2 lists the line identifications and equivalent width measurements in the X-shooter spectra. The observations of NLTT 10480 were originally presented in Kawka & Vennes (2011).

Table 2. Line identifications

Ion	λ (Å)	E.W. (mÅ)		
		NLTT		
		1675	6390	11393
Fe I	3440.606	148	141	...
Fe I	3565.379	38 :	48	...
Fe I	3570.097	80	109	...
Fe I	3581.195	185	161	...
Fe I	3608.859	84 :	...	...
Fe I	3618.768	97 :	...	...
Fe I	3631.463	104 :	95	...
Fe I	3647.842	...	46	...
Fe I	3719.935	117	191	...
Fe I	3734.864	150	119	...
Fe I	3737.131	128	105	...
Fe I	3745.561	112	108	...
Fe I	3748.262	...	50	...
Fe I	3749.485	71 :	106	...
Fe I	3758.233	53	72	...
Fe I	3798.511	46	...	...
Fe I	3815.840	42 :	29 :	...
Fe I	3820.425	115	117	...
Fe I	3825.880	46	63	...
Mg I	3832.304	96 :	60 :	...
Fe I	3834.222	42	...	...
Mg I	3838.292	58 :	91 :	...
Fe I	3859.911	119	77	...
Ca II	3933.663	1161	485	420
Al I	3944.006	48 :	...	...
Al I	3961.520	36 :	...	...
Ca II[1]	3968.469	866	499	420
Fe I	4045.813	56	...	...
Ca I	4226.728	73	...	...
Fe I	4383.544	51	31	...
Ca II	8542.09	64	...	...
Ca II	8662.14	45	...	...

(1) Blended with weak Hϵ.

Table 3. Photometric and astrometric properties of the sample

NLTT	V[1] (mag)	J[2] (mag)	$\mu_\alpha \cos\delta$ [3] (mas yr^{-1})	μ_δ [3] (mas yr^{-1})
1675[4]	17.73 ± 0.04	16.56 ± 0.13	203 ± 6	−100 ± 6
6390	17.33 ± 0.04	16.36 ± 0.13	440 ± 6	−213 ± 6
11393	17.16 ± 0.04	16.04 ± 0.08	250 ± 6	−239 ± 6
23966	17.13 ± 0.04	16.54 ± 0.11	−160 ± 6	−51 ± 6

(1) This work; *V*-magnitude for NLTT 1675 estimated from SDSS *ugriz* photometry. (2) 2MASS, Skrutskie et al. (2006). (3) rNLTT, Salim & Gould (2003). (4) Also known as LSPM J0031+2218, Lépine & Shara (2005).

2.2. Photometry

We searched for photometric measurements using VizieR. The Two Micron All Sky Survey (2MASS) listed infrared *JHK* magnitudes, but only the *J* magnitude was of acceptable quality. For NLTT 6390, 11393 and 23966 we used the acquisition images from the X-shooter observations to estimate a *V* magnitude. The X-shooter acquisition images for NLTT 1675 were unusable. To set the zero point for these magnitudes we used 11 acquisition images of Feige 110 obtained between UT 2010 Dec 10 and 2011 Jan 1. We employed the atmospheric extinction table of Patat et al. (2011).

For NLTT 1675, we also attempted to measure a V magnitude from the EFOSC2 acquisition images, however both acquisition images appear to have been taken through thin clouds and the final magnitudes are unreliable. Fortunately, Sloan Digital Sky Survey (SDSS) photometry is available for NLTT 1675 and we have used these measurements to determine a V magnitude: We obtained a best fit model spectrum to SDSS photometry and then we convolved this model with the V bandpass (Bessell, 1990) providing us with an estimate of the V magnitude.

Table 3 lists the photometric and proper motion measurements for each star.

3. Analysis

3.1. Model atmospheres and spectral syntheses

We extended our grid of model atmospheres for cool hydrogen-rich white dwarfs employed in Kawka & Vennes (2011) to encompass the effective temperature range $4\,900 \leq T_{\rm eff} \leq 8\,000$ K in 100 K steps and the surface gravity range $7.0 \leq \log g \leq 8.75$ in steps of 0.25 dex. The models are in convective and radiative equilibrium. Again, all relevant species (H, H^+, H_2, H_2^+, H_3^+) are included in the statistical equilibrium equation, with electrons contributed by identifiable trace elements (e.g., calcium) included in the charge conservation equation. However, in warmer models that are relevant to the present study ($T_{\rm eff} \geq 6\,000$) electrons are contributed mostly by the ionization of hydrogen atoms. The H_2-H and H-H collision-induced absorptions in the far Lyα wing (see Kowalski & Saumon, 2006) are included using opacity tables from Rohrmann et al. (2011). Synthetic colours as well as detailed hydrogen and heavy element line profiles are computed using the model structures. Table A.1 lists some photometric properties of these models. The colour indices at shorter wavelengths are effected by the Lyα collision-induced absorptions.

The calculation of synthetic hydrogen line profiles deserves further attention. The FWHM for resonant levels computed by Ali & Griem (1965, 1966), the AG formalism, assuming "resonance" interaction ($\propto R^{-3}$) is

$$\Gamma_{3,u} \equiv \frac{w}{N} = 4.8624 \times 10^8 \left(\frac{g_l}{g_u}\right)^{1/2} \frac{f_{lu}}{\nu_{lu}}, \quad (1)$$

where, for example, the lower (l) and upper (u) levels were taken as 1s and 2p in Ali & Griem (1965, 1966), with $g_l/g_u = 1/3$ and the oscillator strength $f_{lu} = 0.4162$, providing a FWHM for the 2p level of 2.4×10^{-8} rad s^{-1} cm^3.

Bergeron et al. (1991) proposed to apply this formalism to principal quantum numbers $l = 1$ and u by taking $g_l/g_u = (l/u)^2$ and f_{lu} as the total oscillator strength between principal quantum numbers $l = 1$ and u. This formalism offers a means to estimate the total width of the level u that includes the s, p, d contributions, i.e., resonant and non-resonant levels. Figure 3 shows Balmer line widths calculated by summing the lower (u) and upper (u') level widths $\Gamma_3 = \Gamma_{3,u} + \Gamma_{3,u'}$. In this formalism, the total width is dominated by the $u = 2$ width, while the contribution of the upper level u' to the width decreases with increasing values of u'.

A comparison with the calculations of Barklem et al. (2000a) for Hα, β, and γ, and Allard et al. (2008) for Hα shows that the total line width is not well represented by this generalisation of the AG formalism. Figure 3 shows that the two formalisms behave differently along the line series. Although the Ali & Griem (1965, 1966) values are nearly constant (when expressed in rad s^{-1}), the width computed by Barklem et al. (2000a) triples

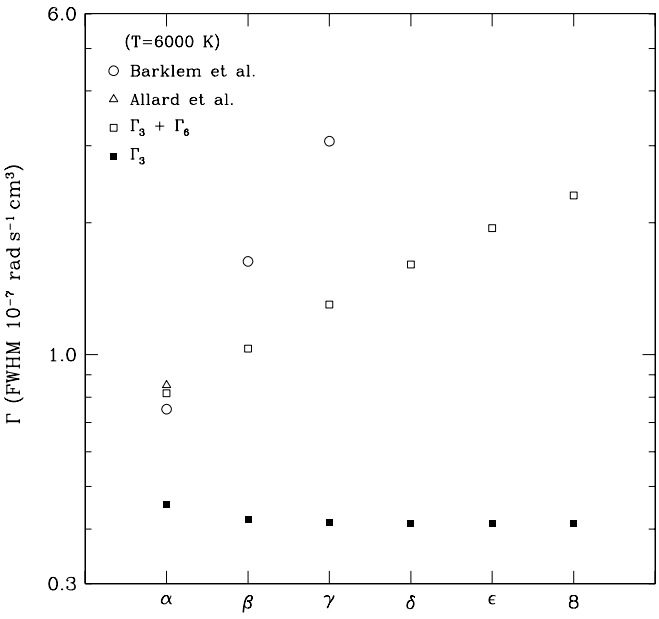

Fig. 3. Self-broadening parameter Γ for members of the Balmer line series. The widths (Γ_3) from Ali & Griem (1965, 1966) follow a markedly different trend than widths from Barklem et al. (2000a). Improvements are obtained by adding a van der Waals term (Γ_6) to Ali & Griem (1965, 1966): $\Gamma_3 + \Gamma_6$.

between Hα and γ. The Ali & Griem (1965, 1966) calculations are dominated by 2p level width and are based on the resonance 1s-2p transition, while the widths tabulated by Barklem et al. (2000a) rely on the np-md formalism for the $n - m$ transition and their calculations employ the "dispersive-inductive" (van der Waals) interaction ($\propto R^{-6}$) in addition to the "resonance" interaction.

Consequently, the AG formalism may be improved by adopting a van de Waals term of the form (see Kurucz & Avrett, 1981)

$$\Gamma_6 \approx 8 \times 10^{-9}\, T_4^{3/10} \left(u^4 - l^4\right)^{2/5}, \quad (2)$$

where $T_4 = T/10^4$. The total line width is then obtained by adding the resonance (Ali & Griem, 1965, 1966) and van der Waals terms: $\Gamma = \Gamma_3 + \Gamma_6$. Figure 3 shows that the resulting line width increases along the series although the widths calculated by Barklem et al. (2000a) remain considerably larger.

Barklem et al. (2000a) also determined validity limits for the quasi-static framework: 35, 13, and 8 Å for Hα, β and γ, respectively, at $T = 4665$ K, revealing potential difficulties with higher members of the Balmer line series.

In order to assess possible systematic errors in the measurement of stellar parameters based on Balmer line profiles, we explored three different approaches for the calculation of Balmer line spectra. In the first approach, the Balmer line profiles from Hα to the series limit are computed using widths from Ali & Griem (1965, 1966) alone, $\Gamma_{\rm AG}$, while in the second approach we combined AG and van der Waals widths, $\Gamma_{\rm AG,vdW}$. In the last approach, the line profiles from Hα to Hγ are computed using widths from Barklem et al. (2000a), $\Gamma_{\rm BPO}$, multiplied by factors of 0.75 and 1.0, again to assess uncertainties, while the upper Balmer lines are computed using $\Gamma_{\rm AG,vdW}$. The Voigt pro-

files including Doppler and self-broadening are convolved with Stark-broadened profiles from Lemke (1997).

3.2. Heavy element line profiles

The dominant broadening mechanism at $\sim$ 6000 K is collision with hydrogen atoms, but the effect of Stark broadening is also included as it contributes significantly at $\sim$ 8000 K.

For broadening of Mg I, Al I, Ca I, and Ca II lines due to collisions with hydrogen atoms we employed the coefficients of Barklem et al. (2000b) where the full-width at half-maximum (FWHM) of the Lorentzian profiles is given by:

$$\frac{w}{n(\mathrm{H\,I})} = \left(\frac{T}{10^4\mathrm{K}}\right)^{(1-\alpha)/2} \Gamma \ \mathrm{rad\,s^{-1}\,cm^3}. \quad (3)$$

For example, we adopted $\log\Gamma = -7.562$ for Ca Iλ4226 and -7.76 for Ca H&K at $T = 10\,000$ K, and $\alpha = 0.238$ for Ca Iλ4226 and 0.223 for Ca H&K. Stark broadening widths for Ca I and Ca II lines were obtained from Dimitrijević & Sahal-Bréchot (1999) and Dimitrijević & Sahal-Bréchot (1992), respectively. Additional parameters (Stark and collisions with hydrogen) were obtained from the compilation of Kurucz & Bell (1995).

Hydrogen molecules provide $\lesssim$20% of the gas pressure in some layers of models at $T_{\rm eff}$ =6000 K and a negligible fraction at 8000 K. Consequently, the effect of collision with molecules is not considered further.

3.3. Effective temperature and surface gravity measurements

Fitting the $V-J$ colour index to synthetic colours (Table A.1) constrains the effective temperature of the cool white dwarfs (Table 4). Within error bars the cooler objects are at $T_{\rm eff} \approx$ 6000 K, while NLTT 23966 is hotter with $T_{\rm eff} \approx$ 7600 K. These preliminary colour-based estimates are corroborated by our detailed Balmer line analysis.

Next, we simultaneously constrained $T_{\rm eff}$ and $\log g$ by fitting the X-shooter spectra with the model grids using χ^2 minimization techniques. All lines up to the series limit, H8/9 for the cooler stars and H10 for NLTT 23966, are included in the analysis, but we excluded the Hϵ/Ca H blend in the three cooler stars. Figure 4 shows the Balmer line profiles of the four white dwarfs compared to the best-fitting model spectra that were calculated using $\Gamma_{\rm AG,vdW}$.

Figure 5 illustrates the range of effective temperatures and surface gravities attained for the sample when employing different broadening parameters. Values connected with thin grey lines were obtained using either $\Gamma_{\rm AG}$ alone (upper points), or $\Gamma_{\rm AG,vdW}$ (lower points). The values connected with full black lines were obtained using $\Gamma_{\rm BPO}$ (Hα,β,γ) combined with $\Gamma_{\rm AG,vdW}$ for the upper Balmer lines (lower points), or reduced $0.75\times\Gamma_{\rm BPO}$ values combined with $\Gamma_{\rm AG,vdW}$ (upper points). The derived parameters are compared to evolutionary cooling tracks (Benvenuto & Althaus, 1999) allowing estimates of the mass and cooling age of each object.

The average mass for the three cooler stars computed using $\Gamma_{\rm AG,vdW}$ line widths is 0.53 $M_\odot$. Similarly, the average mass is 0.57 $M_\odot$ using the combination $\Gamma_{\rm BPO}\times 0.75/\Gamma_{\rm AG,vdW}$. On the other hand, the average mass of 0.96 $M_\odot$ obtained using $\Gamma_{\rm AG}$ appears improbably high, while the average mass of 0.44 $M_\odot$ obtained using the combination $\Gamma_{\rm BPO}/\Gamma_{\rm AG,vdW}$ appears improbably low. Higher (lower) values of the surface gravity (hence density) are derived as a compensation for using smaller (larger) values of Γ. Considering the uncertainties in Γ, it seems appropriate to adopt an average mass near 0.6 $M_\odot$ (see Tremblay et al., 2010) for the three cooler stars.

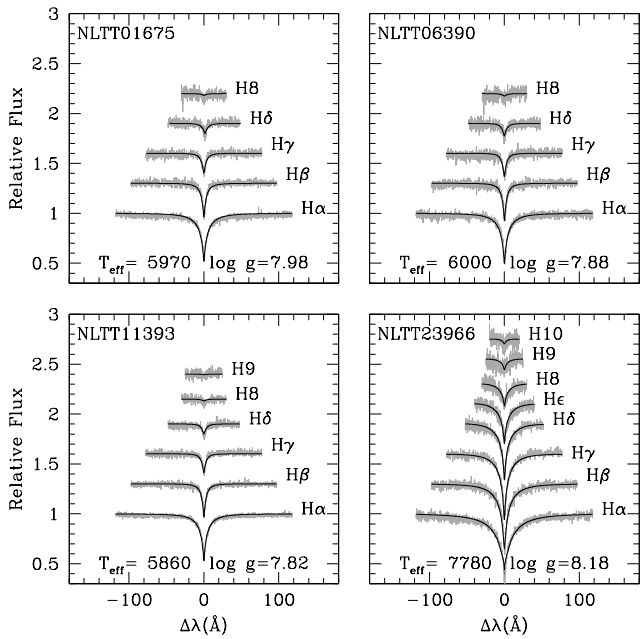

Fig. 4. Balmer line fits of X-shooter spectra using the line-broadening prescription $\Gamma_{\rm AG,vdW}$ (see text). With the exception of NLTT 23966, the Hϵ/Ca H blend is excluded from the line fitting.

Table 4. Stellar properties

NLTT	$T_{\rm eff}$ $(V-J)$ (K)	$T_{\rm eff}$ [1] (K)	$\log g$ [1] (cm s^{-2})	Mass ($M_\odot$)
1675	5800 ± 300	6020 ± 50	8.04 ± 0.07	0.61 ± 0.04
6390	6200 ± 300	6040 ± 40	7.90 ± 0.07	0.53 ± 0.04
11393	5800 ± 300	5890 ± 30	7.86 ± 0.06	0.51 ± 0.03
23966	7600 ± 300	7790 ± 30	8.20 ± 0.04	0.72 ± 0.03

[1] Average of the parameters determined using Balmer line profiles computed using $\Gamma_{\rm AG,vdW}$ and $\Gamma_{\rm BPO}\times 0.75$ models.

On the other hand, the surface gravity, hence mass, of NLTT 23966 is only marginally affected by variations in the self-broadening Γ value because of the dominant effect of Stark broadening at higher temperatures. The higher than average mass estimated for NLTT 23966 may also be attributed to the approximate treatment of convection in current model calculations (Tremblay et al., 2011).

Table 4 lists the adopted effective temperature and surface gravity of the cool white dwarfs. As a compromise, we adopted the average of the values obtained using model spectra calculated with $\Gamma_{\rm AG,vdW}$ or $\Gamma_{\rm BPO}\times 0.75$. Individual white dwarf masses were calculated following Benvenuto & Althaus (1999).

3.4. Abundance of heavy elements

The abundances were computed at $\log g = 8.0$ and $T_{\rm eff} = 6000 \pm 100$ K for the cooler stars, and at $\log g = 8.25$ and $T_{\rm eff} = 7800 \pm 100$ K for NLTT 23966. Table 5 lists the measurements obtained by fitting the spectra with models of varying composition; the quoted errors include the (mild) effect of vary-

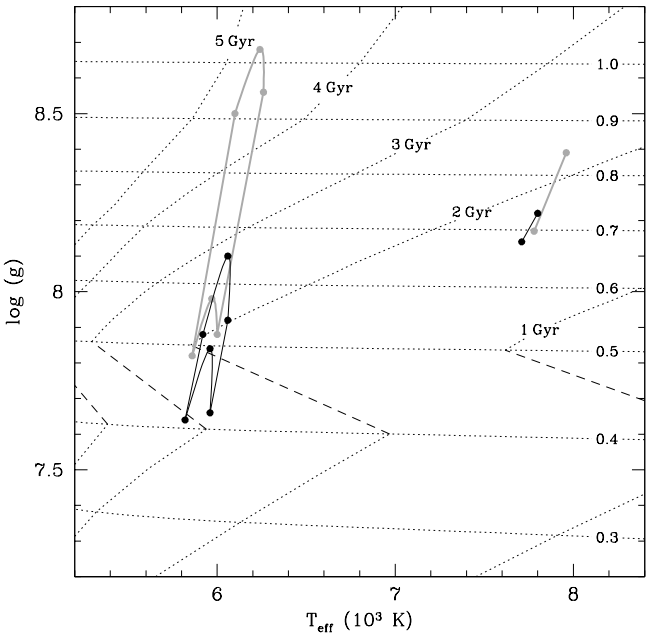

Fig. 5. Range of parameters ($T_{\rm eff}$ vs. $\log g$) determined for a sample of four cool hydrogen-rich white dwarfs using three different prescriptions for hydrogen line broadening (see text). The measured parameters are compared to evolutionary tracks from Benvenuto & Althaus (1999) with masses ranging from 0.3 to 1.0 $M_{\odot}$, and ages ranging from 1 to 5 Gyr. An age discontinuity is apparent $\sim 0.45\,M_{\odot}$ because of the different core composition adopted for models with $M \leq 0.4\,M_{\odot}$ (He) and $M \geq 0.5\,M_{\odot}$ (C/O).

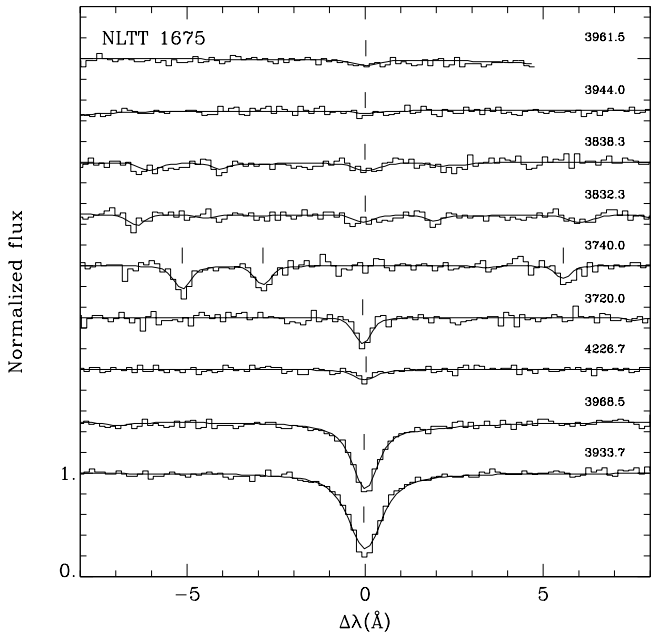

Fig. 6. X-shooter spectra of NLTT 1675 compared to the best fit model. The wavelength scale is centred on the values indicated on the right. The top two spectra show the weak Al I lines, followed by spectra showing Mg I lines around 3838 Å and 3832 Å and Fe I lines around 3740 Å and 3720 Å. Finally, the bottom three spectra show the Ca I and Ca II lines.

Table 5. Abundance measurements [1]

NLTT	log Mg/H	log Al/H	log Ca/H	log Fe/H
1675	−8.56±0.12	−9.28±0.17	−9.53±0.03	−8.63±0.13
6390	−8.66±0.20	< −9.2	−10.00±0.04	−8.57±0.11
11393	< −8.7	< −9.4	−10.24±0.04	< −9.4
23966	...	...	< −10.4	...

(1) Error bars are 1σ and the upper limits are given at 99% confidence.

ing the temperature by ±100 K, and the upper limits are taken at 99% certainty (2.6σ). However, the magnesium and aluminium abundances are based on $\sim 2\sigma$ detections and higher signal-to-noise ratio spectra are required to help improve the measurements. On the other hand, a strict upper limit on the calcium abundance in NLTT 23966 shows that its atmosphere is devoid of heavy elements. Figure 6 shows the various metal lines detected in NLTT 1675 compared to the best fitting model spectra.

3.5. Radial velocity measurements, kinematics, and ages

We measured radial velocities $v_r = 15.0, 83.2, 64.2$ and $66.4\,{\rm km\,s^{-1}}$ for NLTT 1675, 6390, 11393 and 23966, respectively. We estimated the error to be $5.0\,{\rm km\,s^{-1}}$ based on the scatter in individual line measurements and the expected precision of a $R \sim 9000$ spectrograph. Taking into account the expected gravitational redshift of the white dwarfs (based on the spectroscopically determined parameters), the actual velocities of the stars are $v = -16.5 \pm 5.8, 58.3 \pm 5.8, 40.9 \pm 5.4$ and $25.4 \pm 5.4\,{\rm km\,s^{-1}}$ for NLTT 1675, 6390, 11393 and 23966, respectively.

Table 6. Age, distance and kinematics

NLTT	Age (Gyr)	M_V (mag)	d (pc)	U, V, W (km s^{-1})
1675	2.2-2.9	14.27±0.11	49±3	−15±6,−44±8, −4±6
6390	1.7-2.3	14.06±0.11	45±2	−37±5,−101±9,−25±8
11393	1.8-2.2	14.13±0.10	40±2	2±5,−72±7, −5±7
23966	1.6-1.9	13.45±0.06	54±2	−23±5,−31±6, −6±6

Table 6 lists the cooling age, absolute magnitude, distance and Galactic space velocities of the sample. The ages were computed using the evolutionary models of Benvenuto & Althaus (1999) and the absolute magnitudes were calculated using our model grid and radii from Benvenuto & Althaus (1999). The photometric distances were calculated using the apparent (Table 3) and absolute (Table 6) Johnson V magnitudes. Finally, the Galactic velocity components UVW were calculated using Johnson & Soderblom (1987). The lag in V suggest that the white dwarfs belong to the old thin disk (Sion et al., 1988; Pauli et al., 2003, 2006).

3.6. Magnetic field strengths

A lack of splitting at the instrument resolution ($R \sim 9000$) imposes a limit on the magnetic field strength. Setting a limit of approximately 1/3 of a resolution element to the putative magnetic broadening of narrow line cores due to Zeeman splitting:

$$\Delta\lambda \equiv k\,B_s \approx \frac{1}{3}\frac{\lambda}{R} \qquad (4)$$

where $k = 4.67 \times 10^{-13}\lambda^2\,g_{\rm eff}$, λ is the wavelength in Å, B_s is the average surface field in G, and $g_{\rm eff}$ is the effective Landé factor

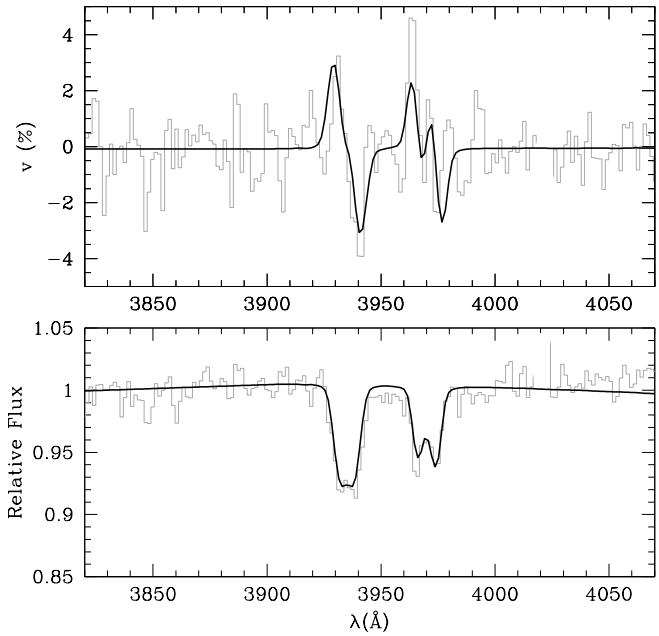

Fig. 7. Circular polarization (*top*) and flux (*bottom*) spectra of NLTT 10480. The observed circular polarization spectrum is compared to a model polarization spectrum at $B_l = 212$ kG (*top*).

(= $\frac{7}{6}$ and $\frac{4}{3}$ for Ca K and H, respectively). For Ca K the resulting limit on the field strength is $B \lesssim 17$ kG. However, this effect could be confused with the effect of stellar rotation.

We obtained VLT/FORS spectropolarimetry for three stars (NLTT 6390, 11393 and 23966) in addition to NLTT 10480. We calculated the mean longitudinal magnetic (B_l in G) field using the weak-field approximation (Angel et al., 1973)

$$k\,B_l = \frac{vF}{dF/d\lambda} \tag{5}$$

where $v = V/I$ is the degree of circular polarization, $F \equiv I$ is the total spectral flux, and $dF/d\lambda$ is the flux gradient. First, we fitted the observed Balmer line profiles with model spectra to determine the best fit line profiles. We then used these line profiles to calculate the flux gradient and determine the longitudinal magnetic field. To measure the longitudinal field strength for NLTT 6390 and NLTT 11393 we used Hβ to Hδ and for NLTT 23966 we used Hα.

Table 7 lists the longitudinal field measurements for three stars (NLTT 6390, 11393 and 23966) from this paper and for the cool white dwarf NLTT 10480 (Kawka & Vennes, 2011). The quoted errors are 1σ. Using the Balmer lines, no fields stronger than $\sim$ 5 to $\sim$ 20 kG are detected in NLTT 6390, 11393 and 23966, but we measured a longitudinal field strength $B_l = -200.4 \pm 124.0$ kG in NLTT 10480, which is barely a 2σ detection. The large uncertainty in B_l is mostly due to the weakness of the Balmer lines (Hβ, γ and δ) in NLTT 10480, but a measurement based on the calcium lines appears more promising.

Equation 5 includes only the first term of a Taylor expansion that is used to calculate v. This is valid where the Zeeman splitting is small compared to the line width. For Ca H&K in NLTT 10480, the Zeeman splitting is fully resolved and therefore we need to include the second term of the Taylor expansion as described in Mathys & Stenflo (1986)

$$v = \frac{1}{F}\left(k\,B_l\,\frac{dF}{d\lambda} + \frac{1}{6}\,(k\,B_l)^3\,\frac{d^3F}{d\lambda^3}\right). \tag{6}$$

By fitting the Ca H&K circular polarization spectrum depicted in Kawka & Vennes (2011) we measured a longitudinal field of -212 ± 50 kG in NLTT 10480. Figure 7 shows the best fit model circular polarization and flux spectra to the observed FORS spectra of NLTT 10480. A reasonable match is achieved between the model and observed spectra, except for the left σ component of the CaII λ3968 Å line, which appears stronger than the model. This is an improvement over the Balmer line measurements, but it still has a significantly larger uncertainty than the measurements obtained for the other white dwarfs in the sample. This is mainly due to the lower signal-to-noise ratio in the spectral region containing the Ca II lines. Combining the measurement of the surface field of 519 ± 4 kG (Kawka & Vennes, 2011) and the Ca H&K measurement of the longitudinal field in NLTT 10480 suggests an inclination below 59°, in agreement with an angle of $60 \pm 3°$ obtained from the strength of the calcium Zeeman-split lines determined in Kawka & Vennes (2011).

Table 7. Magnetic field measurements

NLTT	B_l (kG)	Lines
6390	-4.8 ± 9.0	Hβ, Hγ, Hδ
10480	-200 ± 124	Hβ, Hγ
	-212 ± 50	Ca H&K
11393	$+7.8 \pm 12.2$	Hβ, Hγ, Hδ
23966	-2.6 ± 3.1	Hα

4. Summary and discussion

We have presented a detailed model atmosphere analysis of high-quality spectroscopy of a sample of cool DA white dwarfs. We show that the atmospheres of NLTT 1675, NLTT 6390, and NLTT 11393 are contaminated with heavy elements. On the other hand we show that, contrary to the DAZ white dwarf NLTT 10480, none of these three new DAZ white dwarfs harbour a magnetic field. We also refined our analysis of the magnetic field in NLTT 10480 and confirm our original results (Kawka & Vennes, 2011).

Figure 8 shows the abundances of iron and calcium relative to hydrogen for a sample of cool DAZ white dwarfs, including those from the present sample, and the corresponding abundance ratio of iron with respect to calcium (Fe/Ca). The published abundance measurements were taken from Zuckerman et al. (2003) and Kawka et al. (2011), and from Farihi et al. (2011), Kawka & Vennes (2011) and Zuckerman et al. (2011) for the three magnetic white dwarfs, G77-50, NLTT 10480 and NLTT 43806, respectively. Table B.1 lists the selected measurements. The Fe/Ca abundance ratio appears to be constant as a function of temperature with an average of <Fe/Ca>= 13.1 and a dispersion of $\sigma = 0.33$ dex. The linear fit to the data excludes NLTT 43806, which has a Fe/Ca abundance ratio of ≈ 1.3 (Zuckerman et al., 2011) making it significantly iron poor compared to the rest of the sample. Similarly, Fe/Al is ≈ 0.6 in NLTT 43806 while it is ≈ 4.5 in NLTT 1675. Both calcium and iron abundances show an increase as a function of temperature, but the scatter of iron abundance measurements ($\sigma \sim 0.31$ dex) is lower than that of calcium ($\sigma \sim 0.95$ dex). It is possible that

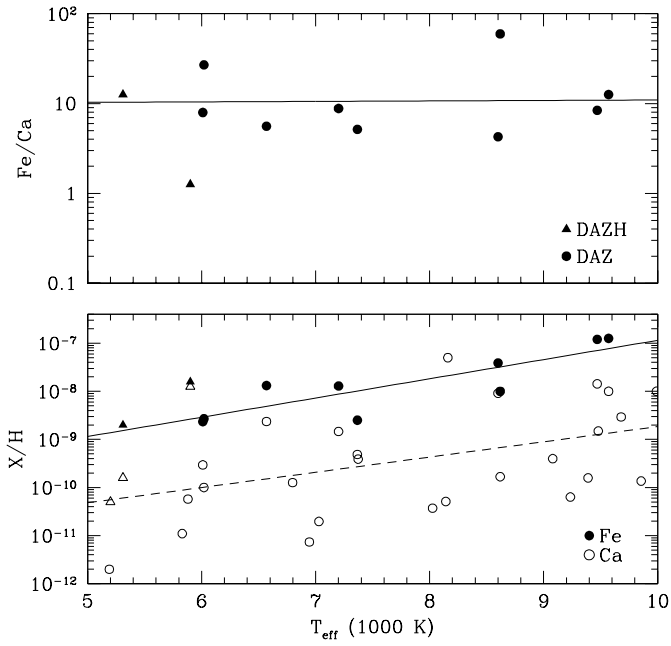

Fig. 8. Abundance ratio of iron with respect to calcium versus the effective temperature (*top*). The best fitting line that excludes NLTT 43806 is also shown. The abundance of iron and calcium versus the effective temperature (*bottom*), upper limits are not shown. The best fitting lines for iron (*full line*) and calcium (*dashed line*) are shown.

Table 8. Inferred accretion rates $\log \dot{M}_X (\mathrm{g\ s^{-1}})$

NLTT	Mg	Al	Ca	Fe
1675	6.59	5.97	5.98	7.17
6390	6.46	<6.02	5.48	7.20
11393	<6.36	<5.76	5.18	<6.31
23966	...	...	<5.08	...

higher signal-to-noise and higher dispersion spectra of objects apparently devoid of iron would uncover even lower iron abundances and thereby increase the scatter in the measurements. In summary, the Fe/Ca abundance fraction is ~10 compared to ≈ 14 in the Sun. The Mg/Ca abundance fraction of NLTT 1675, NLTT 6390, G77-50 and NLTT 43806 range between ≈ 6 and ≈ 30.

We calculated the presumed accretion rates assuming steady state between accretion and diffusion for magnesium, aluminium, calcium and iron. We used the diffusion timescales and mass of the convective zone of Koester (2009). For aluminium we used the diffusion timescale $\log \tau_{\mathrm{Al}} = 4.23$ that Zuckerman et al. (2011) adopted for NLTT 43806, which is a star with temperature and surface gravity similar to our sample of DAZ white dwarfs. Table 8 lists the accretion rates for the NLTT 1675, 6390 and 11393. For objects with upper limits on abundances, such as NLTT 23966, we list the corresponding upper limits on accretion rates. The observed abundance ratios relative to calcium in meteorites (C1 chondrites) or in the Sun (Grevesse et al., 2007) are $\log \mathrm{Mg/Ca}, \log \mathrm{Al/Ca}, \log \mathrm{Fe/Ca} =$ 1.23, 0.10, and 1.15, respectively. Our sample appears to conform with these ratios. Following sample trends, magnesium and iron may well be present in NLTT 11393 but slightly below detection limits in our spectra.

Considering the whole sample, the observed calcium and iron abundances follow the excepted temperature trend assuming a constant accretion rate over cooling ages (see Koester & Wilken, 2006), although it appears somewhat steeper. The calcium and iron abundances increase by 0.32 and 0.4 dex per 1000 K interval, respectively, compared to predicted increases of 0.26 and 0.27 dex per 1000 K interval assuming uniform accretion over the sample. This steeper trend suggests that the accretion flow onto white dwarfs may be slightly abating with time, or that the actual particle flux at the bottom of the convection zone may be underestimated in cooler, i.e., older white dwarfs.

Prior to this study, five DAZ white dwarfs with $T_{\mathrm{eff}} \lesssim 6000\,\mathrm{K}$) were known where two of these, NLTT 43806 (Kawka & Vennes, 2006) and NLTT 10480 (Kawka & Vennes, 2011) were discovered as part of our spectroscopic observations of white dwarf candidates from the rNLTT catalogue. In this paper we add three more cool DAZ white dwarfs to this important sample of accreting objects. Also notable is the high incidence of magnetism among this small sample of stars: Three out of the eight DAZ white dwarfs cooler than ≈ 6000 K (G77-50, NLTT 43806 and NLTT 10480) are weakly magnetic. This incidence is markedly higher than previously estimated (Kawka et al., 2007; Liebert et al., 2003).

Acknowledgements. S.V. and A.K. are supported by GA AV grant numbers IAA300030908 and IAA301630901, respectively, and by GA ČR grant number P209/10/0967. A.K. also acknowledges support from the Centre for Theoretical Astrophysics (LC06014). We thank the referee, D. Koester, for helpful suggestions. This research has made use of the VizieR catalogue access tool, CDS, Strasbourg, France. This publication makes use of data products from the Two Micron All Sky Survey, which is a joint project of the University of Massachusetts and the Infrared Processing and Analysis Center/California Institute of Technology, funded by the National Aeronautics and Space Administration and the National Science Foundation.

References

Ali, A. W., & Griem, H. R. 1965, Physical Review , 140, 1044
Ali, A. W., & Griem, H. R. 1966, Physical Review , 144, 366
Allard, N. F., Kielkopf, J. F., Cayrel, R., & van't Veer-Menneret, C. 2008, A&A, 480, 581
Angel, J. R. P., McGraw, J. T., & Stockman, H. S., Jr. 1973, ApJ, 184, L79
Barklem, P. S., Piskunov, N., & O'Mara, B. J. 2000a, A&A, 363, 1091
Barklem, P. S., Piskunov, N., & O'Mara, B. J. 2000b, A&AS, 142, 467
Benvenuto, O. G., & Althaus, L. G. 1999, MNRAS, 303, 30
Berger, L., Koester, D., Napiwotzki, R., Reid, I. N., & Zuckerman, B. 2005, A&A, 444, 565
Bergeron, P., Wesemael, F., & Fontaine, G. 1991, ApJ, 367, 253
Bessell, M. S. 1990, PASP, 102, 1181
Dimitrijević, M. S., & Sahal-Bréchot, S. 1992, Bull. Astron. Belgrade, 145, 83
Dimitrijević, M. S., & Sahal-Bréchot, S. 1999, A&AS, 140, 191
Dufour, P., Bergeron, P., Schmidt, G. D., et al. 2006, ApJ, 651, 1112
Farihi, J., Dufour, P., Napiwotzki, R., & Koester, D. 2011, MNRAS, 413, 2559
Graham, J. R., Matthews, K., Neugebauer, G., Soifer, B. T. 1990, ApJ, 357, 216
Grevesse, N., Asplund, M., & Sauval, A. J. 2007, Space Sci. Rev., 130, 105
Johnson, D. R. H., & Soderblom, D. R. 1987, AJ, 93, 864
Kawka, A., & Vennes, S. 2006, ApJ, 643, 402
Kawka, A., & Vennes, S. 2011, A&A, 532, A7
Kawka, A., Vennes, S., Dinnbier, F., Cibulková, H., & Németh, P. 2011, American Institute of Physics Conference Series, 1331, 238
Kawka, A., Vennes, S., Schmidt, G. D., Wickramasinghe, D. T., & Koch, R. 2007, ApJ, 654, 499
Kawka, A., Vennes, S., & Thorstensen, J. R. 2004, AJ, 127, 1702
Koester, D. 2009, A&A, 498, 517
Koester, D., Provencal, J., Shipman, H. L. 1997, A&A, 230, L57
Koester, D., Rollenhagen, K., Napiwotzki, R., Voss, B., Christlieb, N., Homeier, D., Reimers, D. 2005, A&A, 432, 1025
Koester, D., Voss, B., Napiwotzki, R., Christlieb, N., Homeier, D., Lisker, T., Reimers, D., & Heber, U. 2009, A&A, 505, 441
Koester, D., & Wilken, D. 2006, A&A, 453, 1051
Kowalski, P.M. & Saumon, D. 2006, ApJ, 651, L137

Kurucz, R.L., & Avrett, E.H. 1981, SAO Spec. Rep., 391
Kurucz R., Bell B., 1995, Atomic Line Data Kurucz CD-ROM No. 23. (Smithsonian Astrophysical Observatory, Cambridge , MA)
Lacombe, P., Wesemael, F., Fontaine, G., & Liebert, J. 1983, ApJ, 272, 660
Lemke, M. 1997, A&AS, 122, 285
Lépine, S., & Shara, M. M. 2005, AJ, 129, 1483
Liebert, J., Bergeron, P., & Holberg, J. B. 2003, AJ, 125, 348
Mathys, G., & Stenflo, J. O. 1986, A&A, 168, 184
Nordhaus, J., Wellons, S., Spiegel, D. S., Metzger, B. D., Blackman, E. G., 2011, Proc. National Academy of Science, 108, 3135
Paquette, C., Pelletier, C., Fontaine, G., Michaud, G. 1986, ApJS, 61, 197
Patat, F., Moehler, S., O'Brien, K., et al. 2011, A&A, 527, A91
Pauli, E.-M., Napiwotzki, R., Altmann, M., et al. 2003, A&A, 400, 877
Pauli, E.-M., Napiwotzki, R., Heber, U., Altmann, M., & Odenkirchen, M. 2006, A&A, 447, 173
Potter, A.T., & Tout, C.A. 2010, MNRAS, 402, 1072
Reid, I. N., Liebert, J., & Schmidt, G. D. 2001, ApJ, 550, L61
Rohrmann, R.D., Althaus, L.G., & Kepler, S.O. 2011, MNRAS, 411, 781
Salim, S., & Gould, A. 2003, ApJ, 582, 1011
Sion, E. M., Fritz, M. L., McMullin, J. P., & Lallo, M. D. 1988, AJ, 96, 251
Skrutskie, M. F., et al. 2006, AJ, 131, 1163
Tremblay, P.-E., Bergeron, P., Kalirai, J. S., & Gianninas, A. 2010, ApJ, 712, 1345
Tremblay, P.-E., Ludwig, H.-G., Steffen, M., Bergeron, P., & Freytag, B. 2011, A&A, 531, L19
Vernet, J., Dekker, H., D'Odorico, S., et al. 2011, A&A, in press (DOI: 10.1051/0004-6361/201117752)
Zuckerman, B., Becklin, E. E. 1987, Nature, 330, 138
Zuckerman, B., Koester, D., Dufour, P., et al. 2011, ApJ, 739, 101
Zuckerman, B., Koester, D., Reid, I. N., Hünsch, M. 2003, ApJ, 596, 477
Zuckerman, B., Reid, I. N. 1998, ApJ, 505, L143

Table A.1. Selected synthetic colours

$\log g$ ($\mathrm{cm\,s^{-2}}$)	$T_{\mathrm{eff}}(K)$ (K)	$B-V$ (mag)	$V-J$ (mag)	$g-J$ (mag)	$g-r$ (mag)	$r-i$ (mag)
7.5	5 800	0.535	1.149	1.428	0.396	0.141
	6 000	0.496	1.070	1.325	0.354	0.119
	6 200	0.463	0.998	1.232	0.316	0.100
	6 400	0.432	0.931	1.145	0.281	0.081
	6 600	0.405	0.867	1.063	0.248	0.063
	6 800	0.380	0.807	0.986	0.218	0.047
	7 000	0.358	0.750	0.913	0.190	0.031
	7 200	0.337	0.695	0.845	0.164	0.017
	7 400	0.319	0.642	0.779	0.140	0.003
	7 600	0.303	0.591	0.716	0.117	−0.011
	7 800	0.289	0.542	0.656	0.095	−0.024
	8 000	0.276	0.494	0.598	0.075	−0.037
8.0	5 800	0.537	1.139	1.419	0.395	0.139
	6 000	0.496	1.061	1.316	0.352	0.118
	6 200	0.463	0.992	1.226	0.314	0.100
	6 400	0.432	0.926	1.140	0.280	0.082
	6 600	0.405	0.863	1.060	0.247	0.065
	6 800	0.380	0.804	0.984	0.218	0.049
	7 000	0.357	0.748	0.912	0.190	0.034
	7 200	0.337	0.694	0.845	0.164	0.019
	7 400	0.319	0.643	0.781	0.141	0.006
	7 600	0.303	0.593	0.720	0.118	−0.007
	7 800	0.289	0.545	0.662	0.098	−0.020
	8 000	0.276	0.499	0.606	0.078	−0.032
8.5	5 800	0.542	1.128	1.409	0.396	0.136
	6 000	0.497	1.050	1.304	0.350	0.116
	6 200	0.461	0.982	1.215	0.311	0.098
	6 400	0.430	0.918	1.131	0.277	0.081
	6 600	0.403	0.857	1.053	0.245	0.065
	6 800	0.378	0.799	0.978	0.215	0.050
	7 000	0.355	0.744	0.908	0.188	0.035
	7 200	0.335	0.691	0.842	0.162	0.021
	7 400	0.316	0.641	0.779	0.139	0.008
	7 600	0.300	0.593	0.720	0.117	−0.004
	7 800	0.286	0.546	0.663	0.097	−0.016
	8 000	0.274	0.501	0.609	0.078	−0.028

Appendix A: Synthetic Johnson and Sloan colours

Table B.1. Abundance measurements of cool white dwarfs.

WD	Name	$T_{\rm eff}$ (K)	log (Ca/H)	log (Fe/H)	Reference
0028+220	NLTT1675	6010	−9.53	−8.63	1
0032−175	G266-135	9235	−10.20	...	2
0151−308	NLTT6390	6020	−10.00	−8.57	1
0208+396	G74-7	7201	−8.84	−7.89	2
0243−026	LHS1442	6798	−9.90	...	2
0245+541	G174-14	5190	−11.70	...	2,3
0315−293[a]	NLTT10480	5200	−10.30	...	4
0322−019[a]	G77-50	5310	−9.8	−8.70	5
0334−224	NLTT11393	5880	−10.24	...	1
0543+579	GD290	8142	−10.29	...	2
0846+346	GD96	7373	−9.41	...	2
1054−226	NLTT25792	8160	−7.30	...	6
1102−183	EC11023-1821	8026	−10.43	...	2
1124−293	ESO439-80	9680	−8.53	...	2
1202−232	EC12028-2316	8619	−9.78	−8.00	2,6
1208+576	G197-47	5830	−10.96	...	2
1225+006	HE1225+0038	9390	−9.8	...	6
1257+278	G149-28	8600	−8.04	−7.41	7
1315−110	HE1315-1105	9080	−9.4	...	6
1344+106	G63-54	6945	−11.13	...	2
1407+425	PG	9856	−9.87	...	2
1455+298	LHS3007	7366	−9.31	−8.60	2,6
1633+433	G180-63	6569	−8.63	−7.55	2
1653+385[a]	NLTT43806	5900	−7.9	−7.80	7
1821−131	LHS3384	7029	−10.71	...	2
1826−045	G21-16	9480	−8.83	...	2
1858+393	G205-52	9470	−7.84	−6.92	2
2115−560	LTT8452	9570	−8.0	−6.90	6
2221−165	HE2221-1630	9990	−8.0	...	6

[a] Magnetic

References. (1) This work; (2) Zuckerman et al. (2003); (3) Berger et al. (2005); (4) Kawka & Vennes (2011); (5) Farihi et al. (2011); (6) Kawka et al. (2011); (7) Zuckerman et al. (2011)

Appendix B: Abundance measurements